

Artificial Neural Networks for Predicting Mechanical Properties of Crystalline Polyamide12 via Molecular Dynamics Simulations

Caglar Tamur[†], Shaofan Li^{†1}, Danielle Zeng[‡]

[†]*Department of Civil and Environmental Engineering, University of California, Berkeley, California, USA*

[‡]*Ford Motor Company, Dearborn, Michigan, USA*

Abstract

Predicting material properties of 3D printed polymer products is a challenge in additive manufacturing due to the highly localized and complex manufacturing process. The microstructure of 3D printed products is fundamentally different from the ones obtained by using conventional manufacturing processes, which makes the task even more difficult. As a first step of a systematic multiscale approach, in this work, we have developed an artificial neural network (ANN) to predict the mechanical properties of the crystalline form of Polyamide12 (PA12) based on data collected from molecular dynamics simulations. Using the machine learning approach, we are able to predict the stress-strain relations of PA12 once the information of the macroscale deformation gradient is provided as the input parameter to the ANN. We have shown that this is an efficient and accurate approach, which can provide a three-dimensional molecular-level anisotropic stress-strain relation of PA12 for any macroscale mechanics model, such as finite element modeling at arbitrary quadrature points.

Keywords: *Molecular dynamics, crystalline polymers, reaxff, polyamide, machine learning, neural network*

1. Introduction

Material modeling of 3D printed material products has been a great challenge for additive manufacturing and other advanced manufacturing technologies. This is because in additive manufacturing, the product is being built on a material point upon a material point, thus the resultant properties are highly dependent on the printing process both spatially and temporally at the localized region.

One of the promising approaches is the multiscale modeling of 3D printed materials [1, 2, 3], which has the ability to extract bottom-up material information to assess the macroscale material properties of a product that is additively manufactured. However, the cost of multiscale modeling may vary, especially when it is involved with molecular scale simulations. Traditionally, in multiscale modeling of crystalline materials, this is overcome by using

¹Email:shaofan@berkeley.edu

a technique called the Cauchy-Born rule [4, 5], which is an approximation of molecular dynamics by using simplified molecular statics. However, for semicrystalline or amorphous materials, because of the lack of a definite crystal structure, full-scale molecular dynamics must be utilized, which will significantly increase the cost of the multiscale simulation. This is because for the macroscale finite element method, it requires a molecular scale stress-strain relation at each material quadrature point for arbitrarily given strain, and it is almost impossible to conduct concurrent molecular dynamics simulations on the fly, unless one has abundant computational resources.

The task at hand is to simulate the molecular-level stress-strain relation under arbitrary strain and temperature with good accuracy, efficiency, and low cost. To solve this problem, in the present work, we adopted the machine learning approach by developing an artificial neural network (ANN) that can predict the molecular level mechanical material properties of polymeric materials. In general, polymeric materials have three different microstructural forms: anisotropic, semicrystalline, and purely amorphous. As a starting point, in this work, we shall first develop an artificial neural network to predict the mechanical properties of the anisotropic crystalline form of polymers.

One of the polymeric materials that is widely used in additive manufacturing is Polyamide12 (PA12), also known as Nylon12, which is a synthetic polymer that is used in many industrial applications such as automobile parts, aerospace applications, medical components, etc. An automotive part manufactured using the Multi Jet Fusion process is shown in Fig. 1.

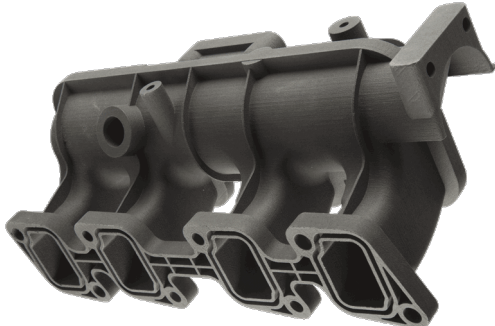


Figure 1: 3D printed Nylon PA12 auto part via HP multi-jet fusion (Courtesy of Ford Motor Company).

PA12 has the chemical formula $[-(\text{CH}_2)_{11}\text{C}(\text{O})\text{NH}-]_n$ as visualized in Fig. 2. In recent years, many 3D printed PA12 products have been fabricated, and they have shown some outstanding material properties. Additively manufactured PA12 is a semicrystalline material, in which the microstructure has a sandwich-like structure of alternating regions of crystal and amorphous zones.

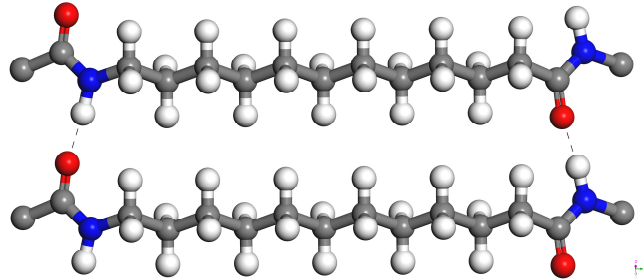


Figure 2: Polyamide12 molecules. Gray, white, blue and red spheres represent carbon, hydrogen, nitrogen and oxygen atoms respectively. Dashed lines indicate the H bonds.

Its structural characterization has been extensively studied since the 1970s with x-ray diffraction (XRD) experiments [6, 7] and with nuclear magnetic resonance (NMR) spectroscopy [8], which revealed that PA12 displays polymorphism and can have crystal phases α , α' , γ and γ' . The most abundant phase is the γ form, which results from slow cooling at atmospheric pressure, whereas the other phases require specific conditions such as rapid quenching and/or high-pressure treatment. For the purposes of our study, we focus on the γ crystal form.

2. Molecular Dynamics Simulations

In this section, we describe the details of molecular dynamics simulations, such as the preparation of initial configurations, the force field selection, and simulation procedures, and we conduct a preliminary study.

2.1. System Setup

We start by constructing the unit cell of the γ form PA12 crystal. The γ phase has a pseudo-hexagonal monoclinic structure with the lattice parameters summarized in Table 1 [6, 7]. Using the atomistic coordinates and the lattice parameters from the experimental literature [7], the unit cell of the γ phase is constructed. This monoclinic structure contains four PA12 chains and is visualized in Fig. 3. Note that the dashed lines indicate hydrogen bonds, and the unit cell is periodic in all directions.

Lattice Parameters	
a	4.79 Å
b	31.90 Å
c	9.58 Å
β	120°
Space Group	P21/C

Table 1: Lattice Parameters for γ form PA12 crystal

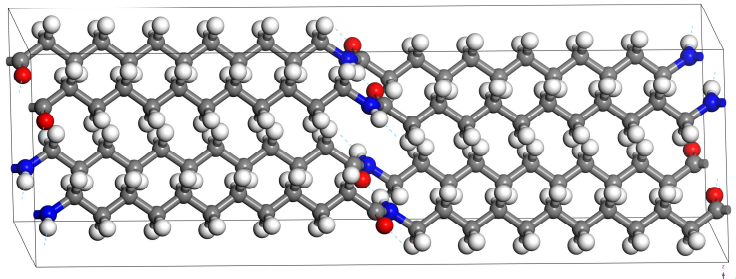


Figure 3: Unit cell of the γ form PA12

Polymer chains are aligned with the y-axis, and the unit cell represents a perfect crystalline system with infinite chain length and no defects. Since MD simulations of triclinic boxes are computationally expensive, we transform the simulation box into an orthogonal cell with chains aligned with the z-axis. Then, the unit cell is duplicated by $(8 \times 4 \times 2)$ in the (x, y, z) directions, respectively, to create a supercell for MD simulations. The resulting model, which consists of around 9,500 atoms, has dimensions $[38.3\text{\AA} \times 33.2\text{\AA} \times 63.8\text{\AA}]$, is visualized in Fig. 4.

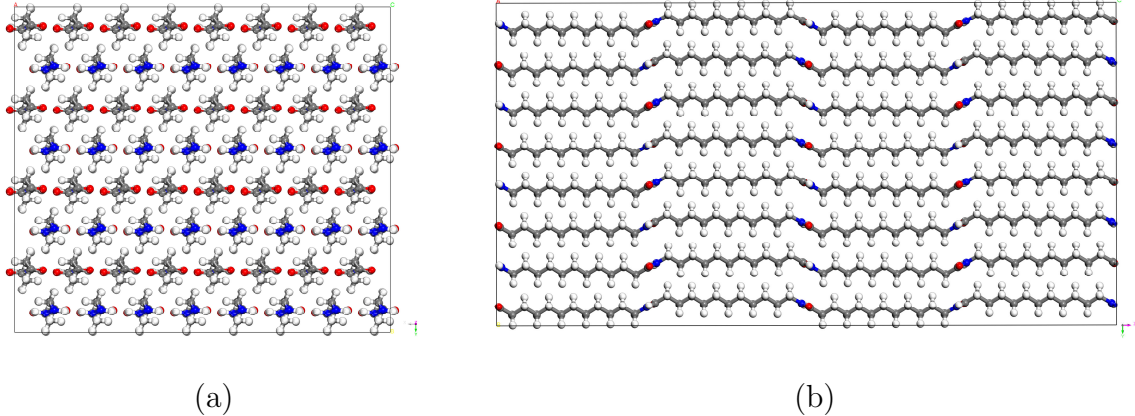


Figure 4: Supercell of perfect PA12 crystals (a) View from x-y plane (b) View from y-z plane.

2.2. Force Field Selection

Force fields represent the interactions between atoms and molecules using a set of equations. In classical forms, force fields consist of empirical potentials that describe bonded interactions (primary bonds, bond angles, and dihedrals) and non-bonded interactions (van der Waals and electrostatic). Choosing a suitable force field for the system under consideration is a crucial part of molecular dynamics simulations.

Several empirical force fields have been used in the simulation of polyamides; some popular examples being OPLS, CVFF, COMPASS, and DREIDING [9]. However, these potentials are typically unable to model chemical reactions and cannot account for bond dissociation. Hence, they are not the ideal choice for investigating the mechanical response of the system in the context of fracture mechanics and rupture of polymer crystals, which may involve the chain scission process [10, 11].

Reactive force fields, on the other hand, have been developed to simulate complex chemical reactions and have been used successfully in deformation simulations that involve bond cleavage. Once such a force field is ReaxFF, originally developed by van Duin [12], which utilizes the so-called bond order formalism to describe chemical bonding. ReaxFF requires no topology information, and it is easy to construct initial MD configurations since only the atomistic coordinates are needed. ReaxFF specially treats weak hydrogen bonds with an explicit energy term in the functional, which plays an important role in polymer systems. The current implementation in LAMMPS utilizes the functional described in [13].

ReaxFF is parameterized for a wide range of materials through quantum mechanical calculations [14] and has also been used in the simulation of polyamide crystals before [15]. For our polymer system, we tested three such parameterizations [16, 17, 18]. The test process involved relaxing the initial structure in the NPT ensemble and comparing the resultant lattice parameters with the experimental values. Among these, the ReaxFF parameterization by Mattson [17] yielded the best result; therefore, it was chosen as the force field for this study.

2.3. Simulation Details and Preliminary Analysis

Molecular dynamics simulations are performed using the Large-Scale Atomic/Molecular Massively Parallel Simulator (LAMMPS) [19]. The simulations are run on Berkeley's high-performance computing cluster Savio using a $[4 \times 2 \times 4]$ CPU grid. MD time steps are chosen as 0.5 fs. Nosé-Hoover thermostat and barostat [20] are used to control temperature and pressure, respectively, with damping parameters chosen as 50 fs and 500 fs.

The initial structure is relaxed in the constant pressure and temperature (NPT) ensemble at 300 K and 1 atm, where the pressure is controlled independently in all directions. We observed that an NPT simulation for 50 ps was sufficient to reach equilibrium, as the lattice parameters stabilized adequately at this point.

As a preliminary study and to investigate in detail the anisotropic mechanical response of PA12 crystals, we constructed a larger MD cell with 38,000 atoms. After relaxation under ambient conditions, we deform the system in different directions under uniaxial tension. Uniaxial deformation is imposed by stretching the unit cell in one direction at a constant strain rate and relaxing the other two dimensions with the NPT ensemble at 1 atm. For this part of the study, we used slower strain rates and deformed the cell quasi-statically in a step-by-step fashion as described in [21]. In this process, the MD cell is deformed to 1% of its final stretch, relaxed in the NVT ensemble, and the stress is sampled and averaged over 5 ps intervals. These steps are repeated until rupture of the polymer chains is observed and the resultant stress-strain behaviors are shown in Fig. 5 for each direction.

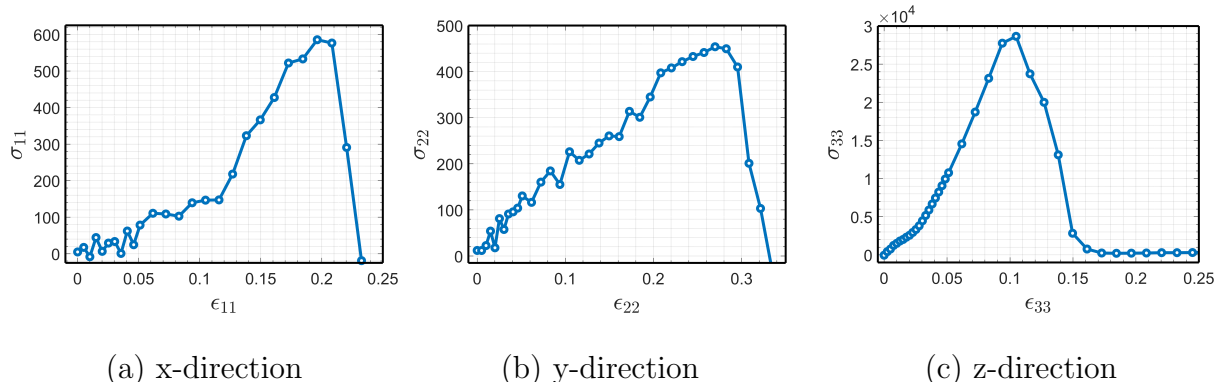


Figure 5: Stress (MPa) versus Strain (engineering) behavior of PA12 in uniaxial tension.

From Fig. 5, we observe that the system is highly anisotropic; crystal is significantly more stiff in the z-direction, which is the direction of polymer chain alignment, and it is more ductile in the other two directions. Interestingly, for the x-direction Fig. 5 (a), there was a remarkable increase in the elastic modulus once the strain reaches around 12%. We investigated this phenomenon to understand whether this is a mechanically induced phase transformation of the crystal. Upon additional analysis, we understand that the process is completely reversible, and the effect disappears once the MD cell is unloaded. Further investigation may be required to draw a final conclusion on the phenomenon.

3. Artificial Neural Network for Constitutive Law

In this section, we present a data-driven approach to model the hyperelastic constitutive law of crystalline PA12, to be used in multiscale mechanics simulations. Our task is to find the mapping between the deformation state and the resulting material response, using the data obtained from the molecular dynamics simulations on an artificial neural network (ANN). We discuss data collection, model selection, training phase, and predictions in detail.

3.1. Data Collection and Processing

In order to generate the data set to train the learning model, we run a total of 720 MD simulations. For the purposes of this study, we limit our attention to uniaxial and biaxial tensile deformation, although the presented methodology is believed to be applicable to any deformation mode. At each simulation, we deform the unit cell in constant strain rate to a predetermined stretch and we average the Virial stress at 50 fs intervals. All MD simulations are run for 4 ps; since the ultimate strain for each direction is different, as seen in Fig. 5, the resultant strain rates vary and cover the ranges presented in Table 2. At the end, we collect a data set that consists of 72,720 data points. Note that the process described here involves remarkably high strain rates and short simulation times, since it was not computationally feasible for us to conduct slower simulations and collect a reasonably large data set at the same time.

	Deformation Direction		
	x	y	z
Ultimate Strain	0.5	0.6	0.15
Strain Rate ($10^{-6}/fs$)	[8.3, 125]	[10, 150]	[2.5, 37.5]

Table 2: Ultimate strain and resulting ranges of strain rates for each direction.

The original data from MD simulations consist of box dimensions $l = \{l_x, l_y, l_z\}$ which can be used to construct the deformation gradient \mathbf{F} and the stress measure we get is the pressure tensor, known as the Virial stress. Virial stress has been shown to be equivalent to continuum Cauchy stress $\boldsymbol{\sigma}$ [22]. In order to adopt the model into the continuum mechanics framework, we need to transform the data set into the tensor quantities utilized in finite deformation. To preserve material objectivity [23, 5], we chose the energetic conjugates right Cauchy-Green tensor \mathbf{C} and the second Piola-Kirchhoff (PK2) stress tensor \mathbf{S} to represent the deformation state and material response, respectively. Each of these second-order tensors have nine components, but making use of the symmetry and Voigt notation we represent them in the vector form as below.

$$\mathbf{C} = [C_{11}, C_{22}, C_{33}, C_{12}, C_{13}, C_{23}] \quad (1)$$

$$\mathbf{S} = [S_{11}, S_{22}, S_{33}, S_{12}, S_{13}, S_{23}] \quad (2)$$

Using the elementary relations of continuum mechanics, we can obtain the \mathbf{C} and \mathbf{S} tensors as follows.

$$J = \det \mathbf{F} \quad (3)$$

$$\mathbf{C} = \mathbf{F}^T \mathbf{F} \quad (4)$$

$$\mathbf{S} = J \mathbf{F}^{-1} \boldsymbol{\sigma} \mathbf{F}^{-T} \quad (5)$$

Now we can state our end goal as finding the map,

$$\Psi : \mathbf{C} \rightarrow \mathbf{S} \quad (6)$$

where Ψ encapsulates the constitutive model that we are going to approximate through supervised learning.

Finally, we normalize our input data set to have a mean of zero and a standard deviation of one, a process known *standardization*. It is common practice in gradient-based learning methods to standardize the data, and it improves the performance of ANNs by helping to solve the convergence issues of the backpropagation algorithm [24, 25]. Standardization can be described as follows.

$$C_{ij}^{std} = \frac{C_{ij} - \hat{\mu}_{ij}}{\hat{\sigma}_{ij}} \quad \text{for } i, j = 1, 2, 3. \quad (7)$$

where C_{ij}^{std} are the normalized components of the right Cauchy-Green tensor, $\hat{\mu}_{ij}$ is the sample mean and $\hat{\sigma}_{ij}$ is the sample standard deviation of the respective component.

3.2. Model Selection and Results

We adopt a feedforward, fully connected network architecture to construct our regression ANN, which may be called a multilayer perceptron (MLP). As shown by the universal approximation theorem, feedforward neural networks can approximate any continuous function, provided that they have at least one hidden layer, have enough neurons, and the activation functions satisfy certain properties [26, 27]. Thus we believe that a MLP is a suitable choice to approximate the hyperelastic constitutive law. Keras [28] Python interface of the TensorFlow [29] machine learning package is used to select and train our ANN model.

Our task is to find an approximation to the constitutive model defined in Eq.(6). Formally, we can express the learning problem as follows.

Find

$$\mathcal{N}(\mathbf{C}, \mathbf{w}) = \hat{\mathbf{S}} \quad (8)$$

such that

$$\mathbf{w} = \underset{\mathbf{w}}{\operatorname{argmin}} \mathcal{L}(\mathbf{S}, \hat{\mathbf{S}}) \quad (9)$$

where \mathcal{N} is encodes the ANN, \mathbf{w} are known as the *weights* of each neuron and \mathcal{L} is a *loss function*. The task in supervised learning is to find optimal weights \mathbf{w} such that the metric defined in the loss function is minimized.

To select the ANN model parameters known as *hyperparameters*, such as the number of hidden layers, number of neurons at each layers, type of activation functions and learning rate of the gradient descent, we conduct hyperparameter optimization. We chose two candidate activation functions which are commonly used in regression, *ReLU* function and its smooth approximate version known as the *Softplus* function.

$$\text{ReLU} : \sigma(x) = \max(x) \quad \text{Softplus} : \sigma(x) = \log(1 + e^x) \quad (10)$$

For the loss function, we choose the mean squared error (MSE) of the PK2 stress, which is defined as

$$\mathcal{L}_{\text{MSE}}(\mathbf{S}, \hat{\mathbf{S}}) = \frac{1}{n} \sum_{i=1}^n \|\mathbf{S}_i - \hat{\mathbf{S}}_i\|_2, \quad (11)$$

where \mathbf{S} is the PK2 stress obtain from MD simulations, $\hat{\mathbf{S}}$ is the predicted stress from ANN and n is the number of data points.

We tried two methodologies to select the best set of hyperparameters, the HyperBand algorithm [30] and Bayesian Optimization with Gaussian Process [31]. Both algorithms will pick the best parameters from a predefined set, which would give the lowest validation loss. The set of parameters that we make the search is determined by preliminary analysis, where the optimizer of the ANN is chosen as the Adam algorithm [32], which implements a version of the stochastic gradient descent (SGD) method. Accordingly, we chose the following range of parameters to perform hyperparameter tuning.

Hyperparameters			
Hidden Layers	Neurons	Activation Function	Learning Rate
[2, 5]	[32, 256]	{ReLU, Softplus}	{ $10^{-1}, 10^{-2}, 10^{-3}$ }

Table 3: Hyperparameter search grid

We start by partitioning the data into a random 20% - 80% train-test split. Then, we run hyperparameter optimization using Hyperband and Bayesian Optimization methods in the domain described in Table 3, leaving aside 20% of the training data to be used to compute validation loss. For all models, the learning rate $\gamma = 10^{-2}$ and the number of hidden layers of four or five gave us the best results. For the rest of the hyperparameters, we investigated the top ten models and chose the ones with the lowest complexity to reduce overfitting. Resulting candidate models are summarized in Table 4.

	Hyperband (1)	Bayesian (2)	Hyperband (3)	Bayesian (4)
Input Layer	6	6	6	6
Hidden Layer 1	$192 \times \text{ReLU}$	$64 \times \text{ReLU}$	$160 \times \text{ReLU}$	$224 \times \text{ReLU}$
Hidden Layer 2	$32 \times \text{Softplus}$	$32 \times \text{Softplus}$	$64 \times \text{Softplus}$	$96 \times \text{Softplus}$
Hidden Layer 3	$32 \times \text{ReLU}$	$256 \times \text{Softplus}$	$32 \times \text{ReLU}$	$64 \times \text{ReLU}$
Hidden Layer 4	$64 \times \text{ReLU}$	$32 \times \text{ReLU}$	$128 \times \text{Softplus}$	$96 \times \text{Softplus}$
Hidden Layer 5	$128 \times \text{ReLU}$	$64 \times \text{ReLU}$	-	-
Output Layer	$6 \times \text{Linear}$	$6 \times \text{Linear}$	$6 \times \text{Linear}$	$6 \times \text{Linear}$
Validation Loss	15630	15026	14109	13538

Table 4: ANN architectures resulting from Hyperband method and Bayesian Optimization

The models summarized above are trained on the train data set for 1000 epochs, and predictions are made on the test data to assess our final performance. The resulting train-test history curves are presented in Fig. 6. We conclude that the ANNs are stable, there is no significant overfitting, and they perform well against the test data set, as seen from the test loss. The best model proves to be ANN-4 and its architecture is schematically visualized in Fig. 7.

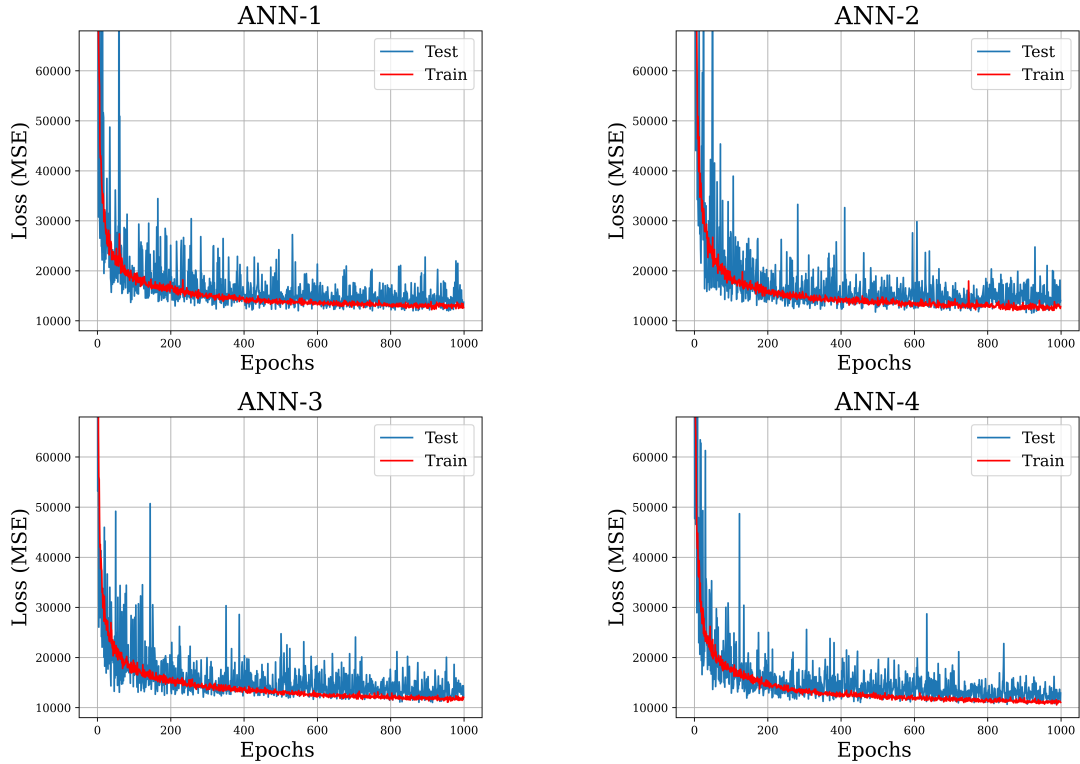


Figure 6: Learning curves of the ANNs: Training and test loss during training phase.

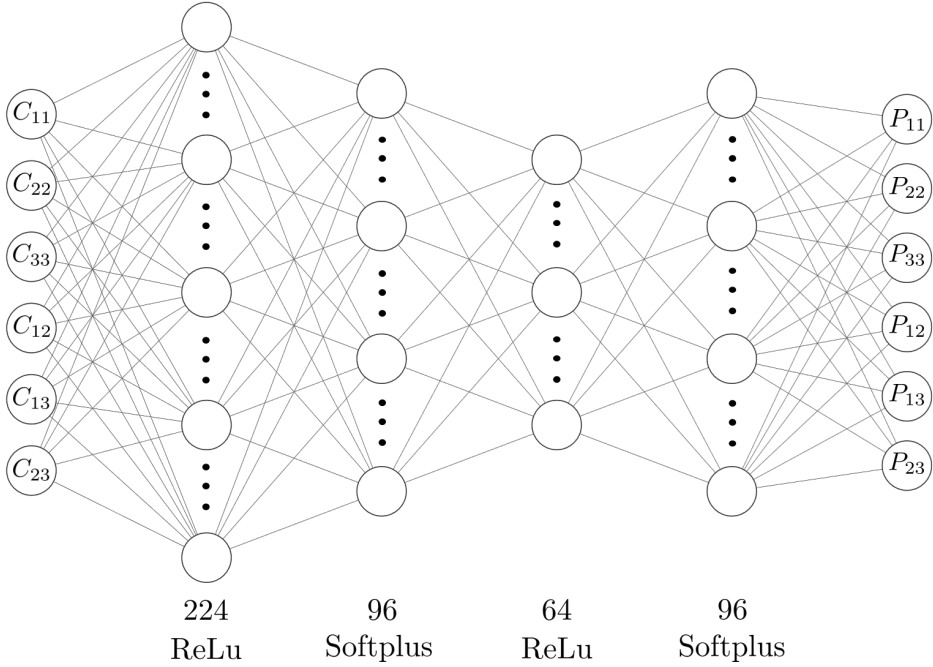


Figure 7: ANN-4 schematic representation [33].

Finally, we tested ANN-4 against a new set of uniaxial tension MD simulations to observe our models performance against variance in strain rate. Two of the simulations used strain rates $\dot{\epsilon}_1 = 20 \times 10^{-6}/fs$ and $\dot{\epsilon}_2 = 30 \times 10^{-6}/fs$ that are within the training interval defined in Table 6. Predictions of ANN-4 is compared with the MD results and the resultant C_{33} versus S_{33} (MPa) relations are shown in Fig. 8.

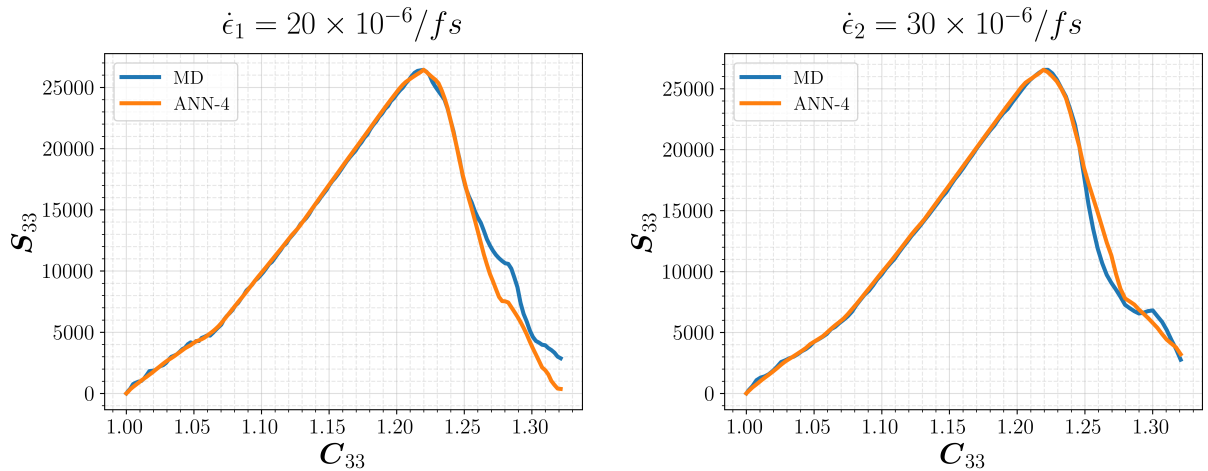


Figure 8: Predictions of ANN-4 for uniaxial tension in z-direction for a new set of simulations. The strain rates are contained in the training range.

Two other MD simulations are considered that utilized strain rates that are beyond the training range in both extremes, namely $\dot{\epsilon}_3 = 1.5 \times 10^{-6}/fs$ (slower) and $\dot{\epsilon}_4 = 50 \times 10^{-6}/fs$ (faster). The resulting predictions are shown in Fig. 9 against the MD results. Although the slower rate resulted in a slightly higher ultimate strength, these results clearly demonstrate the predictive power and robustness against different strain rates of the ANN.

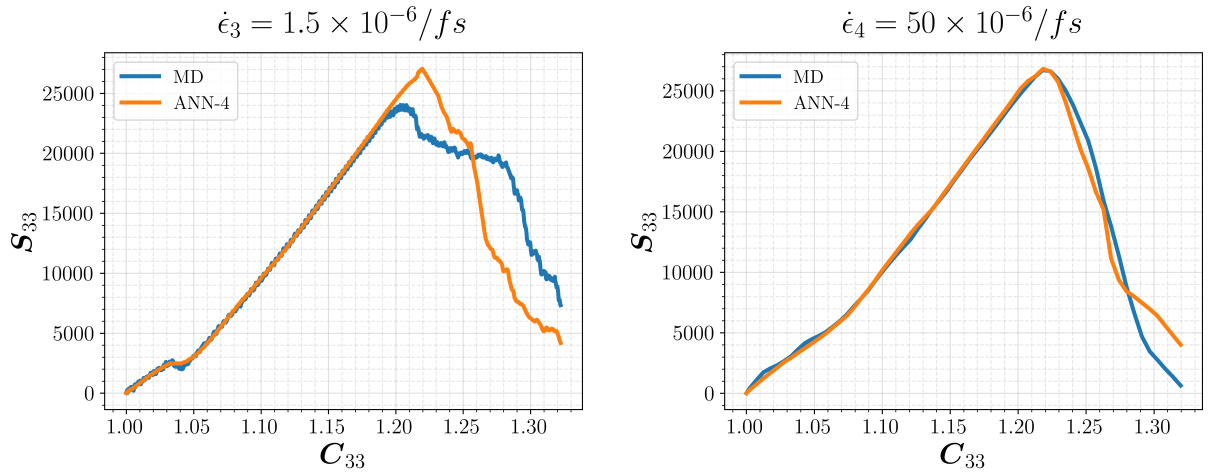


Figure 9: Predictions of ANN-4 for uniaxial tension in z-direction for a new set of simulations. The strain rates are beyond the range of training data.

4. Conclusion and Future Perspectives

In this study, we have developed an artificial neural network to model the mechanical response of crystalline polymers based on molecular dynamics. Initial configurations are generated to model PA12 in γ crystal form. ReaxFF was our choice for the force field, and MD simulations are performed under uniaxial and biaxial tension to generate a data set for the learning model.

ANN architecture is selected through hyperparameter tuning algorithms and carefully calibrated using the training set. The training and validation process produced the best model to be ANN-4, which is proven to be robust and accurate with no significant overfitting. The best model is tested against different strain rates, which covers above and beyond the range of training set. The results proved the predictive power of our approach, even with strain rates that are much slower or faster than the original data.

There are some caveats that need further attention. As found in Section 2.3, there may be a mechanically induced phase transformation of PA12, which may depend on the particular 3D printing processes and the process parameters such as temperature and printing speed. Second, we only considered uniaxial and biaxial tension deformations. For general loads, such as pure shear, compression, and torsion loads, the artificial neural network will need more data and the associated ML training process may become more complicated. Finally, for demonstration purposes, we focused on the fully crystalline form of PA12. However, actual 3D printed material parts consist of semicrystalline structures in which the microstructure has both amorphous and crystalline regions. It is also worth noting that we may need to consider larger MD cells with slower strain rates to simulate more accurate and realistic situations. These issues will be further investigated in the future and will be reported in a separate study.

5. Acknowledgements

We acknowledge the support from the University Grant by Ford Motor Company. Caglar Tamur gratefully acknowledges the financial support for his graduate studies and research by the Fulbright Scholarship Program.

References

- [1] D. López Barreiro, J. Yeo, A. Tarakanova, F.J. Martin-Martinez, and M.J. Buehler. Multiscale modeling of silk and silk-based biomaterials a review. *Macromolecular bioscience*, 19(3):1800253, 2019.
- [2] S. Sharafi, M.H. Santare, J. Gerdes, and S.G. Advani. A multiscale modeling approach of the fused filament fabrication process to predict the mechanical response of 3d printed parts. *Additive Manufacturing*, 51:102597, 2022.
- [3] M. Jamshidian, N. Boddeti, D.W. Rosen, and O. Weeger. Multiscale modelling of soft lattice metamaterials: Micromechanical nonlinear buckling analysis, experimental verification, and macroscale constitutive behaviour. *International Journal of Mechanical Sciences*, 188:105956, 2020.
- [4] S. Urata and S. Li. Higher order cauchy born rule based multiscale cohesive zone model and prediction of fracture toughness of silicon thin films. *International Journal of Fracture*, 203:159–181, 2017.
- [5] Dana Bishara and Shaofan Li. A machine-learning aided multiscale homogenization model for crystal plasticity: application for face-centered cubic single crystals. *Computational Mechanics*, pages 1–17, 2023.
- [6] Gianna Cojazzi, Annamaria Fichera, Carmine Garbuglio, Viscardo Malta, and Roberto Zannetti. The crystal structure of polylauryllactam (nylon 12). *Die Makromolekulare Chemie: Macromolecular Chemistry and Physics*, 168(1):289–301, 1973.
- [7] Kazuo Inoue and Sadao Hoshino. Crystal structure of nylon 12. *Journal of Polymer Science: Polymer Physics Edition*, 11(6):1077–1089, 1973.
- [8] Lon J Mathias and C Greg Johnson. Solid-state nmr investigation of nylon 12. *Macromolecules*, 24(23):6114–6122, 1991.
- [9] Sanjay Krishna, I Sreedhar, and Chetan M Patel. Molecular dynamics simulation of polyamide-based materials—a review. *Computational Materials Science*, 200:110853, 2021.
- [10] Luís Antonio Pinheiro, Marcelo Aparecido Chinelatto, and Sebastião Vicente Canevarolo. The role of chain scission and chain branching in high density polyethylene during thermo-mechanical degradation. *Polymer Degradation and Stability*, 86(3):445–453, 2004.
- [11] Firas Awaja, Shengnan Zhang, Manoj Tripathi, Anton Nikiforov, and Nicola Pugno. Cracks, microcracks and fracture in polymer structures: Formation, detection, autonomic repair. *Progress in Materials Science*, 83:536–573, 2016.
- [12] Adri CT Van Duin, Siddharth Dasgupta, Francois Lorant, and William A Goddard. Reaxff: a reactive force field for hydrocarbons. *The Journal of Physical Chemistry A*, 105(41):9396–9409, 2001.
- [13] Kimberly Chenoweth, Adri CT Van Duin, and William A Goddard. Reaxff reactive force field for molecular dynamics simulations of hydrocarbon oxidation. *The Journal of Physical Chemistry A*, 112(5):1040–1053, 2008.
- [14] T.P. Senftle, S. Hong, M. M. Islam, S. B. Kylasa, Y. Zheng, Y. K. Shin, C. Junkermeier, R. Engel-Herbert, M. J. Janik, H. M. Aktulga, et al. The reaxff reactive force-field: development, applications and future directions. *npj Computational Materials*, 2(1):1–14, 2016.
- [15] Quanpeng Yang, Wenjun Li, Spencer T Stober, Adam B Burns, Manesh Gopinadhan, and Ashlie Martini. Molecular dynamics simulation of the stress–strain behavior of polyamide crystals. *Macromolecules*, 54(18):8289–8302, 2021.
- [16] Małgorzata Kowalik, Chowdhury Ashraf, Behzad Damirchi, Dooman Akbarian, Siavash Rajabpour, and Adri CT Van Duin. Atomistic scale analysis of the carbonization process for c/h/o/n-based polymers with the reaxff reactive force field. *The Journal of Physical Chemistry B*, 123(25):5357–5367, 2019.
- [17] Thomas R Mattsson, J Matthew D Lane, Kyle R Cochrane, Michael P Desjarlais, Aidan P Thompson, Flint Pierce, and Gary S Grest. First-principles and classical molecular dynamics simulation of shocked polymers. *Physical Review B*, 81(5):054103, 2010.
- [18] Weiwei Zhang and Adri CT Van Duin. Improvement of the reaxff description for functionalized hydrocarbon/water weak interactions in the condensed phase. *The Journal of Physical Chemistry B*, 122(14):4083–4092, 2018.
- [19] Aidan P Thompson, H Metin Aktulga, Richard Berger, Dan S Bolintineanu, W Michael Brown, Paul S Crozier, Pieter J in't Veld, Axel Kohlmeyer, Stan G Moore, Trung Dac Nguyen, et al. Lammps-

a flexible simulation tool for particle-based materials modeling at the atomic, meso, and continuum scales. *Computer Physics Communications*, 271:108171, 2022.

[20] Denis J Evans and Brad Lee Holian. The nose–hoover thermostat. *The Journal of chemical physics*, 83(8):4069–4074, 1985.

[21] Dundar E Yilmaz and Adri CT van Duin. Investigating structure property relations of poly (p-phenylene terephthalamide) fibers via reactive molecular dynamics simulations. *Polymer*, 154:172–181, 2018.

[22] Arun K Subramaniyan and CT Sun. Continuum interpretation of virial stress in molecular simulations. *International Journal of Solids and Structures*, 45(14–15):4340–4346, 2008.

[23] Faisal As’ad, Philip Avery, and Charbel Farhat. A mechanics-informed artificial neural network approach in data-driven constitutive modeling. *International Journal for Numerical Methods in Engineering*, 123(12):2738–2759, 2022.

[24] Y. LeCun, L. Bottou, G. B. Orr, and K. Müller. Efficient backprop. In *Neural networks: Tricks of the trade*, pages 9–50. Springer, 2002.

[25] J. Sola and J. Sevilla. Importance of input data normalization for the application of neural networks to complex industrial problems. *IEEE Transactions on nuclear science*, 44(3):1464–1468, 1997.

[26] Kurt Hornik, Maxwell Stinchcombe, and Halbert White. Multilayer feedforward networks are universal approximators. *Neural networks*, 2(5):359–366, 1989.

[27] Kurt Hornik. Approximation capabilities of multilayer feedforward networks. *Neural networks*, 4(2):251–257, 1991.

[28] François Chollet et al. Keras, 2015.

[29] Martín Abadi, Ashish Agarwal, Paul Barham, Eugene Brevdo, Zhifeng Chen, Craig Citro, Greg S. Corrado, Andy Davis, Jeffrey Dean, Matthieu Devin, Sanjay Ghemawat, Ian Goodfellow, Andrew Harp, Geoffrey Irving, Michael Isard, Yangqing Jia, Rafal Jozefowicz, Lukasz Kaiser, Manjunath Kudlur, Josh Levenberg, Dandelion Mané, Rajat Monga, Sherry Moore, Derek Murray, Chris Olah, Mike Schuster, Jonathon Shlens, Benoit Steiner, Ilya Sutskever, Kunal Talwar, Paul Tucker, Vincent Vanhoucke, Vijay Vasudevan, Fernanda Viégas, Oriol Vinyals, Pete Warden, Martin Wattenberg, Martin Wicke, Yuan Yu, and Xiaoqiang Zheng. TensorFlow: Large-scale machine learning on heterogeneous systems, 2015. Software available from tensorflow.org.

[30] L. Li, K. Jamieson, G. DeSalvo, A. Rostamizadeh, and A. Talwalkar. Hyperband: A novel bandit-based approach to hyperparameter optimization. *The Journal of Machine Learning Research*, 18(1):6765–6816, 2017.

[31] T. O’Malley, E. Bursztein, J. Long, F. Chollet, H. Jin, L. Invernizzi, et al. Kerastuner, 2019.

[32] Diederik P Kingma and Jimmy Ba. Adam: A method for stochastic optimization. *arXiv preprint arXiv:1412.6980*, 2014.

[33] Alexander LeNail. Nn-svg: Publication-ready neural network architecture schematics. *J. Open Source Softw.*, 4(33):747, 2019.